The Journal of Immunology

Negative Regulation of MAVS-Mediated Innate Immune Response by PSMA7

Yongxia Jia, Ting Song, Congwen Wei, Caifei Ni, Zirui Zheng, Quanbin Xu, Hongfang Ma, Li Li, Yanhong Zhang, Xiang He, Yang Xu, Wei Shi and Hui Zhong

J. Immunol. 2009;183;4241-4248; originally published online Sep 4, 2009;
doi:10.4049/jimmunol.0901646
http://www.jimmunol.org/cgi/content/full/183/7/4241

The Journal of Immunology is published twice each month by The American Association of Immunologists, Inc., 9650 Rockville Pike, Bethesda, MD 20814-3994.

Print ISSN: 0022-1767 Online ISSN: 1550-6606.

Negative Regulation of MAVS-Mediated Innate Immune Response by PSMA7[1]

Yongxia Jia,[2]* Ting Song,[2]* Congwen Wei,[2]* Caifei Ni,* Zirui Zheng,* Quanbin Xu,* Hongfang Ma,* Li Li,* Yanhong Zhang,* Xiang He,† Yang Xu,‡ Wei Shi,[3]‡ and Hui Zhong[3]*

Innate immunity to viruses involves receptors such as Retinoic Acid Induced Gene-1 (RIG-I), which senses viral RNA and triggers a signaling pathway involving the outer mitochondrial membrane protein mitochondrial antiviral signaling (MAVS). Recent work has identified that NLRX1, a member of another class of innate immune receptors, sequesters MAVS away from RIG-I and thereby prevents mitochondrial antiviral immunity. In this study, we demonstrate that the proteasome PSMA7 (α4) subunit associates with MAVS in vivo and in vitro. Expression of PSMA7 results in a potent inhibition of RIG-1 and MAVS-mediated IFN-β promoter activity; conversely, depletion of PSMA7 with small interference RNA enhances virus-induced type I IFN production, with consequent reduction of virus replication. Furthermore, a striking reduction in the abundance of endogenous MAVS with overexpressed PSMA7 was found and virus infection leads to transient increase in the endogenous PSMA7 protein level. Cumulatively, these results suggest that PSMA7 is a negative regulator of the MAVS-mediated innate immunity that probably serves to attenuate the establishment of an antiviral state during viral infection, highlighting the biological significance of PSMA7-MAVS association as an important cellular regulatory control. *The Journal of Immunology,* **2009, 183: 4241–4248.**

The innate immune system can rapidly detect invading pathogenic microbes and eliminate them (1–3). Among the best characterized receptors in the innate immune system are the TLRs, NOD-like receptors (NLRs),[4] and Retinoic Acid Induced Gene-1 (RIG-I)-like receptors (4–10). RIG-I contains tandem N-terminal caspase recruitment domains (CARDs) that interact with the CARD domains of MAVS to induce IFNs (11–19). Recently, another NOD-like receptor, NLRX1, has been identified, which is located in mitochondria and appears to act as a negative regulator of RIG-I by sequestering MAVS to prevent RIG-I signaling (20). However, the mechanism by which the IFN pathway is negatively regulated is still poorly understood.

The 26S proteasome complex is a ubiquitous protease complex composed of two large complexes: the 20S catalytic core complex and the 19S regulatory complex. The 19S complex is required for the recognition of poly-ubiquitinated protein substrates that are degraded inside of the 20S core complex. The barrel-shaped 20S particle is made up of four rings, each of which contains seven different subunits. The two inner rings contain β-type subunits and the outer rings comprise α-type subunits (21–25). The PSMA7 subunit of 20S proteasome is located on the outer ring of the proteasome complex and plays a key role in proteasomal activity regulation. Certain findings suggest PSMA7 interaction with its partners can target these partners for proteasome-dependent degradation. Cho et al. (26) showed that PSMA7 interacts with hypoxia-inducible factor-1α and targets hypoxia-inducible factor-1α for proteasome-dependent degradation. Human hepatitis B virus X protein, another binding partner of PSMA7, is also quickly degraded by the proteasome pathway (27, 28). Because proteasome subunits can be exchanged with exogenous subunits in vivo and in vitro (29–32), PSMA7 may have a role in recruiting specific substrates to the proteasome complex by subunit exchanging and proteasome assembling.

The present study demonstrates that PSMA7 physically interacts with MAVS and inhibits the ability of MAVS to induce type I IFN, suggesting an important yet novel regulatory mechanism from NLRX1 in MAVS functions.

Materials and Methods

Cell culture, transfections, and small interfering RNA (siRNA)

HEK293, MCF-7, and murine embryonic fibroblasts cells were grown in DMEM (Invitrogen) supplemented with 10% heat-inactivated FBS (HyClone), 2 mM L-glutamine, 100 U/ml penicillin, and 100 mg/ml streptomycin. Transient transfections were performed with Lipofectamine 2000 (Invitrogen) according to the manufacturer's instructions.

For stable down-regulation of PSMA7 or PSMA4, cells were transfected with pU6-PSMA7-siRNA or pU6-PSMA4-siRNA using Lipofectamine 2000 (Invitrogen) and selected in the presence of G418 3 days after transfection. G418-resistant single cell clones were amplified and screened by Western blot with anti-Flag Ab (Sigma-Aldrich). Two independent clones for each construct were harvested and used for additional experiments. The selection of the coding sequences for siRNA was based on previous guidelines. Each sequence was analyzed using the NCBI-BLAST database to verify that there was no homology greater than 15/21 residues with other genes. The sequences for the siRNA-encoding regions for PSMA7 and PSMA4 were obtained from GenBank Accession No. DQ890589 (nucleotides 324–342, http://www.

*State Key Laboratory of Pathogen and Biosecurity, Beijing Institute of Biotechnology, Beijing, China; †Institute of Disease Control and Prevention, Beijing, China; and ‡Key Laboratory for Molecular Enzymology and Engineering, Ji Lin University, Changchun, China

Received for publication June 1, 2009. Accepted for publication July 27, 2009.

The costs of publication of this article were defrayed in part by the payment of page charges. This article must therefore be hereby marked *advertisement* in accordance with 18 U.S.C. Section 1734 solely to indicate this fact.

[1] This work was supported in part by National Natural Science Foundation (30772605, 30700413, 30870500, and 30871276) and by the Beijing Natural Science Foundation (7092081).

[2] Y.J., T.S., and C.W. contributed equally to this work.

[3] Address correspondence and reprint requests to Drs. Hui Zhong and Wei Shi, Beijing Institute of Biotechnology, Beijng, China. E-mail addresses: towall@yahoo.com and shiw@jlu.edu.cn

[4] Abbreviations used in this paper: NLR, NOD-like receptor; CARD, caspase recruitment domain; siRNA, small interfering RNA; MOI, multiplicity of infection; VSV, vesicular stomatitis virus; UPS, ubiquitin-proteasome system; RIG-I, Retinoic Acid Induced Gene-1; MAVS, mitochondrial antiviral signaling; HA, hemagglutinin.

www.jimmunol.org/cgi/doi/10.4049/jimmunol.0901646

ncbi.nlm.nih.gov/nuccore/124126866? report = GenBank) and GenBank Accession No. DQ895750 (nucleotides 218–236, http://www.ncbi.nlm.nih.gov/nuccore/123998148? report = GenBank). siRNA oligos directed at the same nucleotides were synthesized and were ligated into pU6 vector (Invitrogen) using BamH1 and *Eco*RI.

Transient knockdown of PSMA7 or PSMA4 was generated by PSMA7 siRNA or PSMA4 siRNA oligonucleotide (Santa Cruz Biotechnology) transfection following the manufacturer's instructions. Scrambled siRNA oligos were used as knockdown control.

Plasmids

Flag-MAVS plasmid was provided by Dr. Zhijian Chen (University of Texas Southwestern Medical Center, Dallas, Texas). Truncated forms of MAVS lacking the CARD-like domain (residues 10–77), the proline-rich region (residues 103–152) or the transmembrane domain (residues 514–535) were cloned into pcDNA3 using overlap extension PCR. Flag-tagged PSMA7 and its mutants were provided by Cheng Cao (Beijing Institute of Biotechnology, China). Plasmids encoding GST fusion proteins were prepared by cloning PCR-amplified fragments into pGEX4T-2 (Amersham Biosciences). GFP-MAVS and RFP-PSMA7 were prepared by cloning PCR-amplified fragments into pDSRed and pEGFP (Biosciences Clontech).

Immunoprecipitation and immunoblot analysis

Cell lysates were prepared in lysis buffer (50 mM Tris-HCl (pH 7.5)/1 mM PMSF/1 mM DTT/10 mM sodium fluoride/10 mg/ml aprotinin/10 mg/ml leupeptin/10 mg/ml pepstatin A containing 1% Nonidet P-40). Soluble proteins were subjected to immunoprecipitation with anti-Flag (Sigma-Aldrich), anti-Myc (Santa Cruz Biotechnology), or anti-mouse IgG Ab (Sigma-Aldrich). An aliquot of the total lysates (5%, v/v) was included as a control. Immunoblot analysis was performed with anti-Myc (Santa Cruz Biotechnology), anti-Flag (Sigma-Aldrich), anti-GFP (Santa Cruz Biotechnology), anti-PSMA7 (Santa Cruz Biotechnology), anti-MAVS (Abcam), or anti-β-Tubulin (Sigma-Aldrich) Ab. The Ag-Ab complexes were visualized by chemiluminescence (PerkinElmer). When necessary, figures were cropped using Adobe Photoshop software (Adobe). Band density was analyzed using Image-Quant software (Amersham Biosciences).

Immunofluorescence assay

Cells were washed briefly in PBS, fixed in 4% paraformaldehyde in PBS for 10 min, and the nuclei were stained for 10 min with 4′6-diamidino-2-phenylindole dihydrochloride. After a final wash in PBS, samples were preserved in glycerol and images were captured using a digital camera under a confocal microscope (Zeiss LSM510).

Protein binding assays

In GST pull-down experiments, cell lysates were incubated for 2 h at 4°C with 5 μg purified GST or GST fusion proteins bound to glutathione beads. The absorbates were washed with lysis buffer and then subjected to SDS-PAGE and immunoblotting analysis. An aliquot of the total lysates (5%, v/v) was included as a loading control on the SDS-PAGE.

Luciferase reporter assays

HEK293 cells were transfected with 0.2 μg of the Luciferase reporter pNF-κB-LUC, IFN-β-LUC, or IRF3-LUC plus 0.02 μg of the internal control reporter pCMV-LacZ, with or without various amounts of MAVS, RIG1-(N) expression vector, poly (dAT: dAT) or poly (I: C). Transfected cells were collected and Luciferase activity was assessed. All experiments were repeated at least three times.

RNA analysis

First-strand cDNA was generated from total RNA using random priming and moloney murine leukemia virus reverse transcriptase (Invitrogen). Real-time PCR was performed using QuantiTect SYBR Green PCR Master Mix (Qiagen) in triplicate experiments and analyzed on an ABI Prism 7700 analyzer (Applied Biosystems). All real-time values were normalized to 18S ribosomal RNA. IFN-β using the following primers: 3′; IFN-β S, 5′-CACGACAGCTCTTTCCATGA-3′; IFN-β AS, 5′-AGCCAGTGCTC GATGAATCT.

Subcellular fractionation

Cells were washed 36 h after transfection in hypotonic buffer (10 mM Tris HCl (pH 7.5)/10 mM KCl/1.5 mM MgCl2/protease inhibitors) and then homogenized in the same buffer by bouncing 20 times. The homogenate was centrifuged at 500 $\times$ *g* for 5 min to remove nuclei and unbroken cells. The supernatant was centrifuged again at 5,000 $\times$ *g* for 10 min to generate membrane pellets containing mostly mitochondria and cytosolic supernatant.

Viral infections

MCF-7 cells were plated in 96-well plates at a density of 1×10^4 cells and incubated overnight. Viral infection was performed when 60% cell confluence was reached. Culture medium was replaced by serum-free DMEM, and VSV was added into the medium at concentration of 80 hemagglutinating units per ml and 5 multiplicity of infection (MOI), respectively. After 1 h incubation, extracellular virus was removed by washing cells two times with serum-containing medium. Cells and supernatant were harvested at indicated times post infection.

In vivo ubiquitination assays

Cells were cotransfected with plasmids expressing increasing amounts of Myc-PSMA7, Flag-MAVS, and hemagglutinin (HA)-tagged ubiquitin. Cells were grown in medium containing MG132 (20 μM) for 6 h. Anti-Flag immunoprecipitates were analyzed by immunoblotting with anti-HA Ab, whole cell lysates were subjected to immunoblotting with anti-Myc and anti-Flag Ab, anti-β-Tubulin was used as equal loading control.

Vesicular stomatitis virus (VSV) infection and plaque assay

MEFs cells were infected with VSV at a MOI of 0.002 for 20 h. Virus yield was measured in culture supernatants collected from VSV-infected MEFs by standard plaque assay. In brief, cells were infected with serial dilutions of recovered viruses for 1 h and were overlaid with DMEM containing 0.5% low melting agarose. After 24 h of incubation, plates were stained with crystal violet and plaques were counted.

Statistical analysis

Analyses were done using the statistical software SAS/STAT (SAS Institute). Data analyses over time were undertaken by repeated measures analysis using SAS/STAT. A value of $p < 0.05$ was considered the threshold value for statistical significance.

Results

PSMA7 interacts with MAVS in vivo and in vitro

Owing to the crucial role of MAVS in the RIG1-MDA5 mediated antiviral response, a search for MAVS-interacting molecules was performed to uncover regulatory components of the pathway. Yeast two-hybrid approaches indicate that PSMA7 associates with MAVS (data not shown). To confirm the yeast two-hybrid analysis, Flag-tagged MAVS and Myc-tagged PSMA7 were transfected into HEK293 cells, and a coimmunoprecipitation experiment was performed (Fig. 1*A*). Myc-tagged PSMA7 was detected in the anti-Flag immunoprecipitation from cells cotransfected with Flag-MAVS, but not with a negative control Flag-tagged protein. This observation substantiates the yeast two-hybrid analysis and establishes an interaction between MAVS and PSMA7. The specificity of the interaction between MAVS and PSMA7 was also confirmed by coimmunoprecipitation analysis using normal serum (IgG). Importantly, endogenous MAVS was found to be specifically coimmunoprecipitated with endogenous PSMA7 (Fig. 1*B*). Moreover, immunofluorescence analysis of HEK293 cells transfected with GFP-MAVS and RFP-PSMA7 showed that the staining patterns of MAVS overlapped partially with PSMA7 (Fig. 1*C*). Because MAVS is a mitochondrial membrane protein, we next examined whether PSMA7 and MAVS colocalized in the same membrane compartment. HEK293 cells were homogenized in an isotonic buffer that preserved mitochondria and other organelles, and the cell lysates were then subjected to differential centrifugation to separate mitochondria and cytosol. Immunoblotting with an Ab against anti-MAVS and anti-PSMA7 showed that the both MAVS and some portion of PSMA7 located in mitochondria compartment, indicating that both proteins localize to mitochondria (Fig. 1*D*).

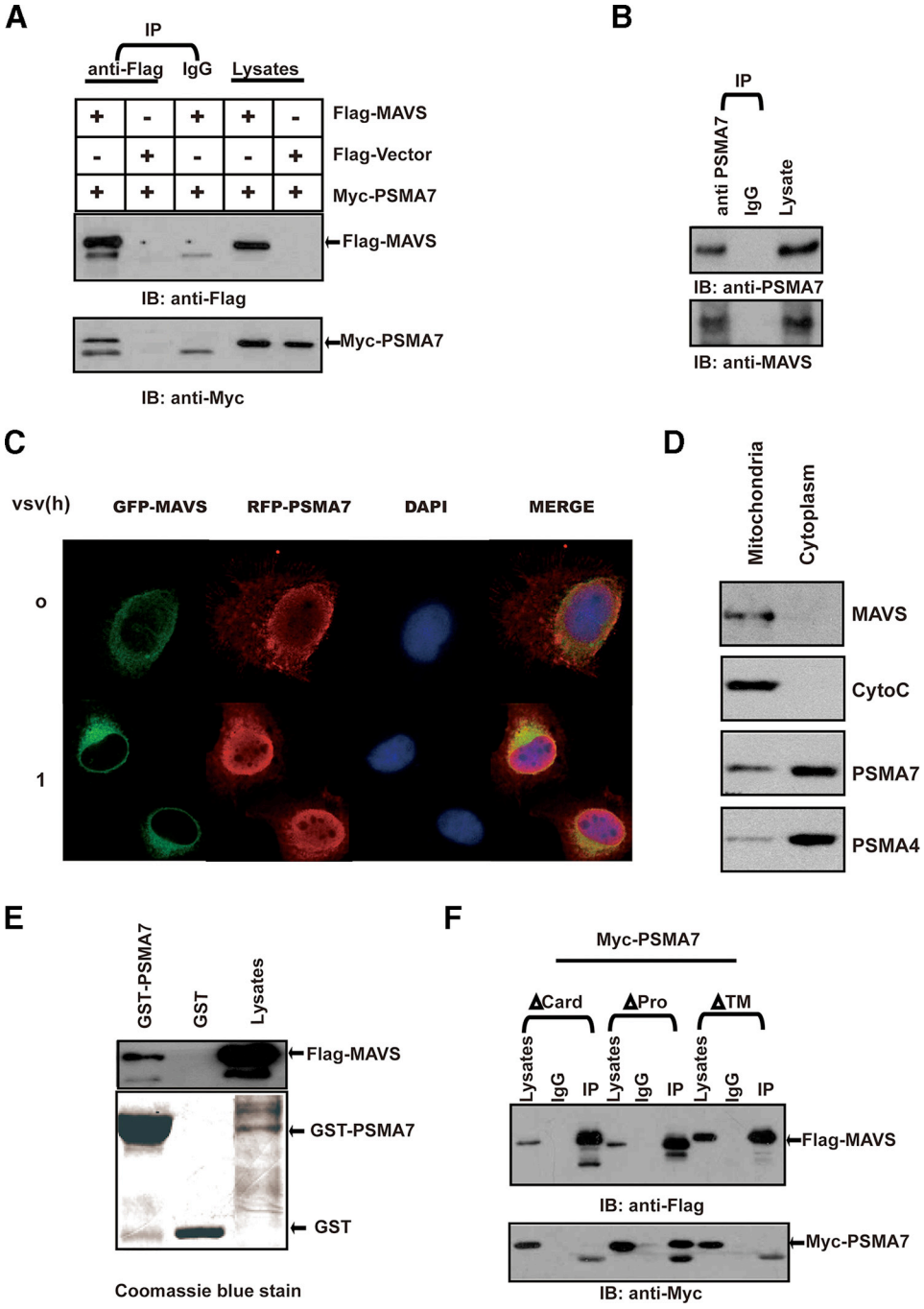

FIGURE 1. PSMA7 associates with MAVS. *A*, HEK293 cells were cotransfected with Flag-MAVS and Myc-PSMA7 expression plasmids or Flag-vector, and anti-Flag or IgG immunoprecipitates were analyzed by immunoblotting with anti-Myc or anti-Flag Ab. *B*, Lysates from HEK293 cells were subjected to immunoprecipitation with anti-PSMA7 or IgG, fractionated by SDS-PAGE, and subsequently analyzed by immunoblotting with anti-MAVS Abs. *C*, HEK293 cells were cotransfected with GFP-MAVS and RFP-PSMA7 expression plasmid with or without VSV infection; immunofluorescence was monitored. DNA was stained with 4′6-diamidino-2-phenylindole dihydrochloride (blue). *D*, Mitochondria and cytoplasm fractions were analyzed by immunoblotting with anti-MAVS, anti-cytochrome C, anti-PSMA7, or anti-PSMA4 Ab. *E*, HEK293 cells were transfected with Flag-MAVS-expressing plasmid. The GST-PSMA7 fusion protein absorbates from cell lysates were analyzed by immunoblotting with anti-Flag Ab (*top*). Loading of the GST proteins was assessed by Coomassie blue staining (*bottom*). *F*, HEK293 cells were cotransfected with Myc-PSMA7 and Flag-MAVS expression plasmids or Flag-MAVS mutants; anti-Flag immunoprecipitates were analyzed by immunoblotting with anti-Myc or anti-Flag Ab.

To demonstrate the interaction of PSMA7 and MAVS in vitro, lysates from HEK293 cells expressing Flag-MAVS were incubated with GST or GST-PSMA7 fusion protein. Analysis of the absorbates by immunoblotting with anti-Flag showed that MAVS bound GST-PSMA7, but not GST (Fig. 1*E*), thus demonstrating an in vitro interaction between PSMA7 and MAVS.

To further map the PSMA7 binding sites in MAVS, three mutants containing truncated forms of MAVS lacking either the CARD-like domain (residues 10–77), the proline-rich region (residues 103–152), or the transmembrane domain (residues 514–535) were constructed and overexpressed together with PSMA7. Fig. 1*F* showed the N-terminal CARD domain and C-terminal TM domain of MAVS are required for MAVS signaling and for the interaction with PSMA7.

PSMA7 inhibits MAVS-mediated induction of IFN-β

To test whether this interaction has functional relevance, the effects of PSMA7 on MAVS-mediated type-I IFN activation were explored directly. Increasing amounts of expression vectors for PSMA7 were cotransfected with the expression construct for MAVS into HEK293 cells together with an IFN-β Luciferase reporter as well as pCMV-LacZ as an internal control. Thirty-six hours after transfection, the luciferase activity was measured and normalized based on β-galactosidase activity. As is shown in Fig. 2*A*, overexpression of MAVS in HEK293 cells potently activates the IFN-β promoter, while as low as 0.4 μg of PSMA7 was sufficient to exert a potent repression of IFN-β response. The extent of repression increased with increasing amounts of expressed PSMA7, suggesting that PSMA7 inhibited the induction of IFN-β by MAVS in a dose-dependent manner.

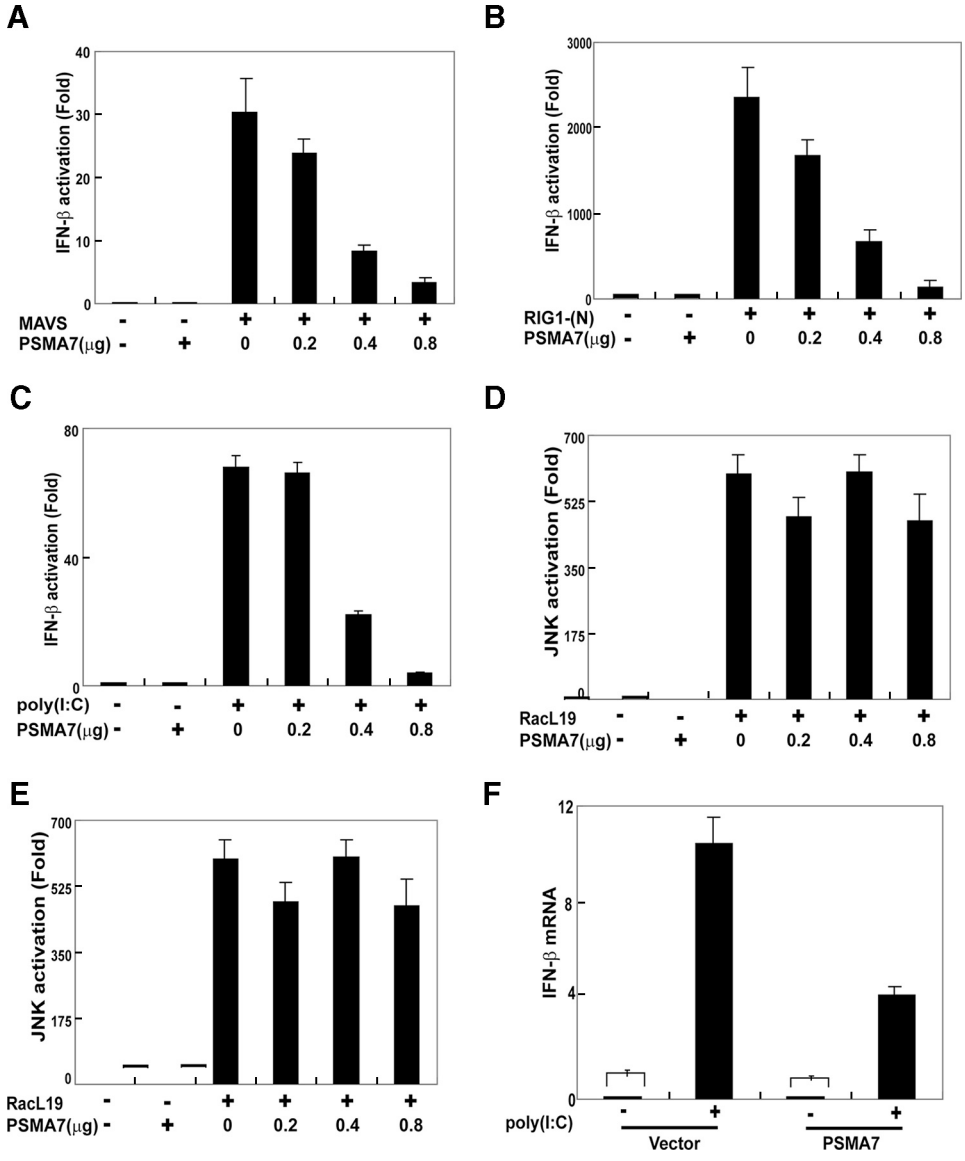

FIGURE 2. PSMA7 inhibits MAVS-mediated activation of IFN-$\beta\beta$. *A*, HEK293 cells were transfected with increasing amounts of PSMA7, MAVS expression vector together with IFN-β-LUC. The LUC activity was measured 24 h later and normalized for transfection efficiency. The error bar represents SD from the mean value of duplicated experiments. *B*, The experiments were conducted as in *A*, except that RIG1-(N) plasmid was transfected in lieu of MAVS. *C*, The experiments were conducted as in *A*, except that poly(I:C) plasmid was transfected in lieu of MAVS. *D*, The experiments were conducted as in *A*, except that RacL19 plasmid and JNK-LUC were transfected in lieu of MAVS and IFN-β-LUC. *E*, The experiments were conducted as in *A*, except that PSMB2 plasmid was transfected in lieu of PSMA7. *F*, HEK293 cells were transfected with PSMA7 and poly(I:C), RNA was extracted 24 h later and IFN-β mRNA was analyzed by quantitative RT-PCR.

Both pathways that activate NF-κB and IRF3 lead to IFN-β transcription. Similar repressions of MAVS-induced activation of NF-κB and IRF3 reporters by PSMA7 were also observed (data not shown).

Overexpression of the tandem N-terminal CARD-like domains of RIG-I (designated as RIGI (N)) also induces IFN-β through MAVS. As is shown in Fig. 2*B*, PSMA7 significantly reduces the ability of RIG-I to activate IFN-β transcription. Signaling in response to the synthetic viral dsDNA analog poly (dAT:dAT) and synthetic viral dsRNA analog poly(I:C) are mediated both at the cell membrane through TLR3 and in the cytoplasm by means of direct binding to the RLH molecules to activate MAVS. We delivered poly(dAT:dAT) and poly(I:C) into the cytoplasm by transfection; PSMA7 also inhibited induction of IFN-β by poly(dAT:dAT) and poly(I:C) in a dose-dependent manner (Fig. 2*C* and data not shown). As a control for specificity, Jnk luciferase reporter activated by racL19 was not affected by PSMA7 (Fig. 2*D*). Other proteasome complex subunit proteins, PSMB2 and PSMA4, did not affect IFN-β luciferase (Fig. 2*E* and data not shown), suggesting the specific negative role of PSMA7 in IFN-β induction. Furthermore, IFN-β mRNA levels reduced sharply in poly(I:C) transfected cells containing the PSMA7 expression plasmid (Fig. 2*F*). Collectively, these data indicate that PSMA7 functions as an inhibitor of RLH-mediated MAVS antiviral signaling.

PSMA7 siRNA enhances VSV induced-IFN-β production

We next investigated the function of endogenous PSMA7 in dsRNA induced IFN-β production. PSMA7 and PSMA4-specific siRNA oligonucleotides, which reduced PSMA7 and PSMA4 protein by ~80% and 90%, were used (Fig. 4*B*). Consistent with the inhibitory effects of PSMA7 on the IFN-β promoter, expression of PSMA7-specific siRNA, but not control siRNA or PSMA4 siRNA, enhanced IFN-β promoter activity substantially by 16 h posttransfection with poly(I:C) (Fig. 3*A*). We then assessed whether endogenous PSMA7 was sufficient to induce the same regulation upon virus infection. IFN-β mRNA and protein levels were quantified in PSMA7 siRNA cells infected with VSV, which activates RIG-I and MAVS for type-1 IFN production. IFN-β mRNA induction by VSV was increased ~3-fold in cells with PSMA7 siRNA compared with control siRNA or PSMA4 siRNA (Fig. 3*B*). Consistent with the transcriptional data, VSV-induced IFN-β protein level was also greater in the infected PSMA7 siRNA cells (Fig. 3*C*). The effect of PSMA7 on IFN-β

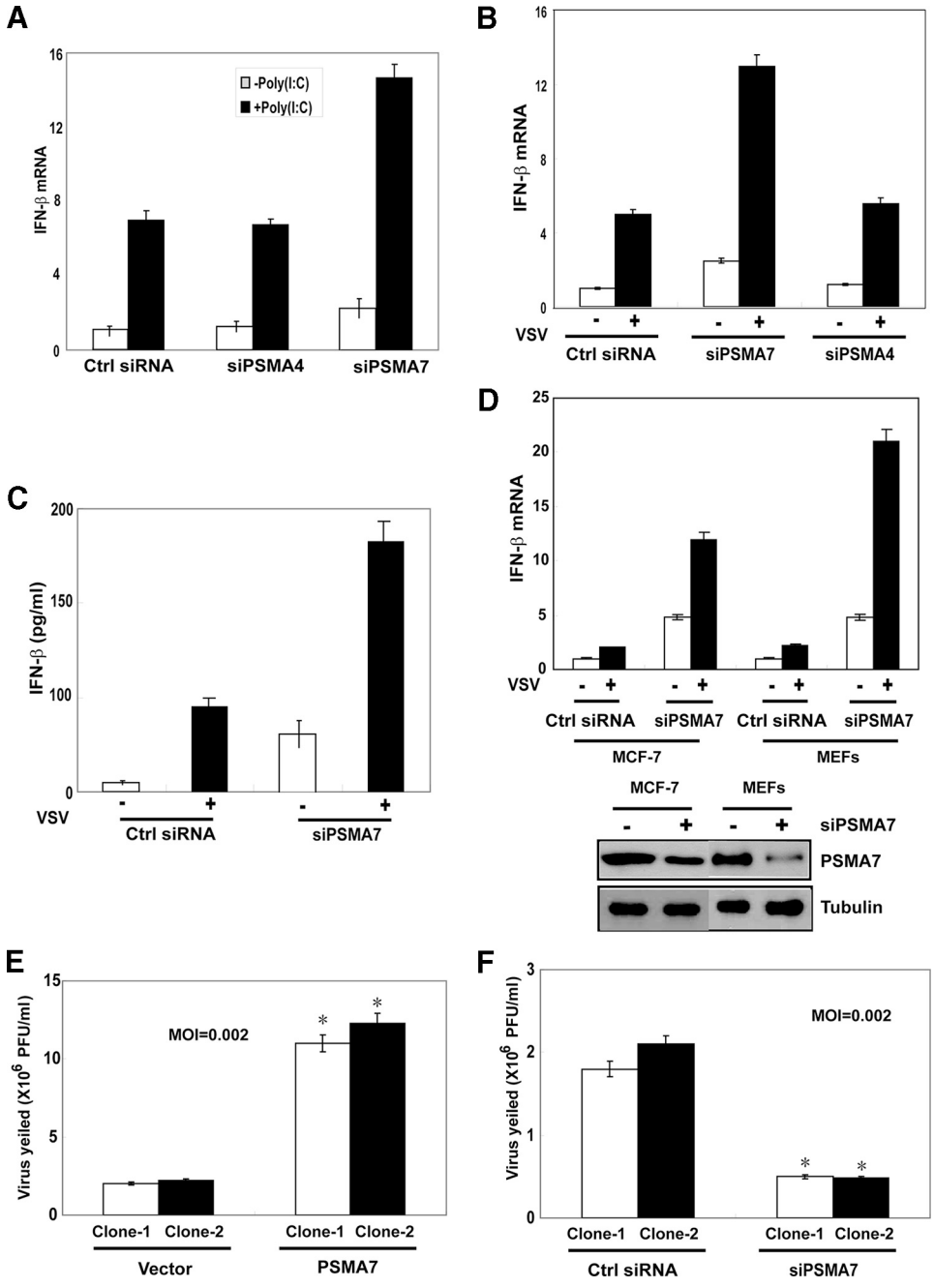

FIGURE 3. PSMA7 siRNAi enhances VSV-induced IFN-β production. *A*, Activation of IFN-β by poly(I:C) in the presence of control or PSMA7, PSMA4-targeted siRNA as measured by quantitative real-time PCR. All results were normalized to 18S rRNA values. Data from *A* are presented as mean $\pm$ SD from three independent experiments. *B*, IFN-β mRNA and *C*, IFN-β protein in VSV-infected HEK293 cells in the presence of control nontargeting or PSMA7-targeted siRNA or PSMA4-targeted siRNA. Data from *B* and *C* are presented as mean $\pm$ SD from three independent experiments. *D*, IFN-β mRNA in VSV-infected MCF7 or MEFs cells in the presence of control nontargeting or PSMA7-targeted siRNA. Data from *D* are presented as mean $\pm$ SD from three independent experiments. *E*, Two stably transfected clones with WT PSMA7 and two stably transfected clones with empty vector in MEFs were infected with VSV at a MOI of 0.002. Virus yield in the supernatants at 20 h after infection was determined by plaque assay. $n = 3$ independent experiments, each done in triplicate. Points, mean; bars, SD. The differences in VSV sensitivity between PSMA7 and the two control clones achieved statistical significance ($p < 0.01$). *F*, Two stably transfected clones with PSMA7 siRNA and two stably transfected clones with control siRNA in MEFs were infected with VSV at a MOI of 0.002. Virus yield in the supernatants at 20 h after infection was determined by plaque assay. $n = 3$ independent experiments, each done in triplicate. Points, mean; bars, SD. The differences in VSV sensitivity between PSMA7 siRNA and the two control siRNA clones achieved statistical significance ($p < 0.01$).

mRNA induction is not restricted to a single cell type, because PSMA7 siRNA also led to increased IFN-β mRNA induction by VSV in MCF-7 cells and MEFs cells (Fig. 3*D*).

We next sought to determine whether PSMA7 regulated replication of VSV, as MAVS-mediated IFN signaling is critical in restricting replication of these RNA viruses. To this end, two PSMA7 expressing stable clones of MEFs cells with two empty vector expressing clones and two PSMA7 siRNA knockdown clones with two control siRNA expressing clones were obtained. Consistent with the suppressive effects of MAVS on RIG-I-mediated IFN signaling (Fig. 2), exogenous expression of PSMA7 increased the production of infectious VSV in the culture supernatants of infected MEFs, whereas interference of PSMA7 expression decreased it (Fig. 3, *E* and *F*). These results provide biological evidence that PSMA7 acts as a negative regulator of RIG-I-mediated type I-IFN signaling and thereby modulates the innate antiviral cellular response.

PSMA7 destabilizes MAVS

To explore the mechanism for the inhibitory effect of PSMA7 on antiviral signaling, we examined the effect of PSMA7 on endogenous MAVS abundance. When expression plasmids encoding PSMA7 were transfected into MCF-7 cells, remarkably, a striking reduction in the abundance of endogenous MAVS with overexpressed PSMA7 was found and this reduction of MAVS by PSMA7 was also dose dependent (Fig. 4*A*). As a control, increasing amounts of PSMA4 expression vector did not change the endogenous MAVS level (data not shown), indicating that the MAVS down-regulation is a specific effect elicited by PSMA7. We next investigated the function of endogenous PSMA7 in MAVS regulation. Expression of PSMA7-specific siRNA, but not control siRNA or PSMA4 siRNA, increased endogenous MAVS abundance in MCF-7 cell line (Fig. 4*B*). Quantitative RT-PCR revealed no change in endogenous MAVS mRNA

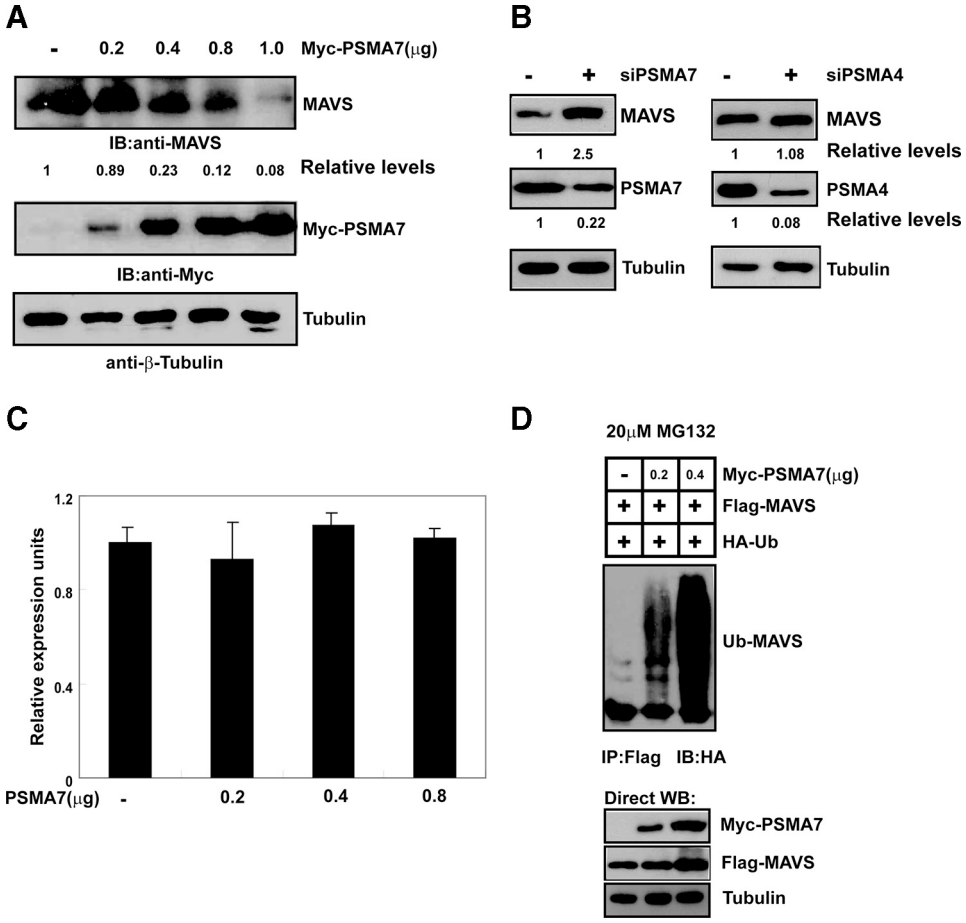

FIGURE 4. PSMA7 promotes MAVS degradation. *A*, MCF-7 cells were transfected with plasmids expressing increasing amount of Myc-PSMA7. Whole cell lysates were analyzed by immunoblotting with anti-MAVS or anti-Myc Ab; anti-β-Tubulin was used as equal loading control. *B*, MCF-7 cells were transfected with siPSMA7 or siPSMA4 oligos, After 24 h, whole cell lysates were analyzed by immunoblotting with anti-MAVS, anti-PSMA7 or anti-PSMA4 Ab; anti-β-Tubulin was used as equal loading control. *C*, MCF-7 cells were transfected with plasmids expressing increasing amount of Myc-PSMA7, RNA was extracted, and MAVS mRNA was analyzed by quantitative RT-PCR. *D*, Increasing amounts (indicated on the top) of Myc-PSMA7 were cotransfected with plasmids encoding Flag-MAVS and HA-tagged ubiquitin. Cells were grown in medium containing MG132 (20 μM) for 6 h. Anti-Flag immunoprecipitates were analyzed by immunoblotting with anti-HA Ab, whole cell lysates were subjected to immunoblotting with anti-Myc and anti-Flag Ab, and anti-β-Tubulin was used as equal loading control.

level, suggesting that PSMA7 down-regulates MAVS by posttranscriptional modification (Fig. 4*C*).

To further delineate the mechanism for the PSMA7-mediated MAVS degradation, HEK293 cells were cotransfected with plasmids expressing Flag-MAVS, increasing amount of Myc-PSMA7 and HA-ubiquitin together with the proteasome inhibitors MG132 (20 μM for 6 h), and MAVS was then immunoprecipitated by an anti-Flag Ab and blotted with an anti-HA Ab. As shown in Fig. 4*D*, PSMA7 led to an increased steady level of MAVS ubiquitination. These results indicate that PSMA7 may have a major role in MAVS ubiquitination and its proteasome-mediated degradation.

Regulation of PSMA7 during virus infection

Negative regulatory proteins can function as negative feedback molecules to attenuate the response or they can function as "brakes" that are removed to allow the response to be enhanced. To investigate which of the above mechanisms applies to PSMA7, we analyzed the PSMA7 expression level in response to VSV infection in MCF-7 cells. As shown in Fig. 5*A*, VSV infection markedly increased the amount of PSMA7 protein as early as 1 h after infection. Moreover, immunofluorescence analysis of HEK293 cells transfected with GFP-MAVS and RFP-PSMA7 followed by VSV infection showed that the staining patterns of PSMA7 and MAVS were intensified by virus infection (Fig. 1*C*). Notably, the increase of PSMA7 persisted and resumed back to its background level 24 h after VSV infection. As a control, the abundance of PSMA4 protein in response to VSV infection remained unchanged. Moreover, we determined whether the presence of PSMA7 disrupted the interaction between Rig1 and MAVS in response to virus infection. Results showed that VSV infection led to enhanced interaction of MAVS and Rig1, while PSMA7 introduction destroyed the increased binding between MAVS and RIG1 (Fig. 5*B*).

Cumulatively, these results suggest that PSMA7 is a negative regulator of MAVS-mediated innate immunity that probably serves to attenuate the establishment of an antiviral state during viral infection, highlighting the biological significance of PSMA7-MAVS association as an important cellular regulatory control. The transient inhibition of the activity of PSMA7 by pharmacological agents might therefore provide a strategy to enhance antiviral responses.

Discussion

Innate immunity to viruses involves receptors such as RIG-I, which senses viral RNA and triggers a signaling pathway involving the outer mitochondrial membrane protein MAVS. Recently, the regulation of MAVS has been cast into the limelight. NLRX1, a member of another class of innate immune receptors, sequesters MAVS away from RIG-I and thereby prevents downstream antiviral signaling emanating from the mitochondria via MAVS (20).

Regulating the stability of MAVS is another potential mechanism to modulate the innate immune response. In this study, we characterized PSMA7 as a novel and essential cofactor for MAVS function in RIG1 signaling. Several lines of findings support this argument. First, PSMA7 was shown to interact directly with MAVS both in vitro and in vivo. Second, overexpression of PSMA7 destabilized MAVS and severely impaired IFN-β activation. The abundance of endogenous MAVS was affected by overexpressed PSMA7, but not by another proteasome subunit PSMA4. Therefore, like HIF1α (17), PSMA7 targets MAVS for proteasome-dependent

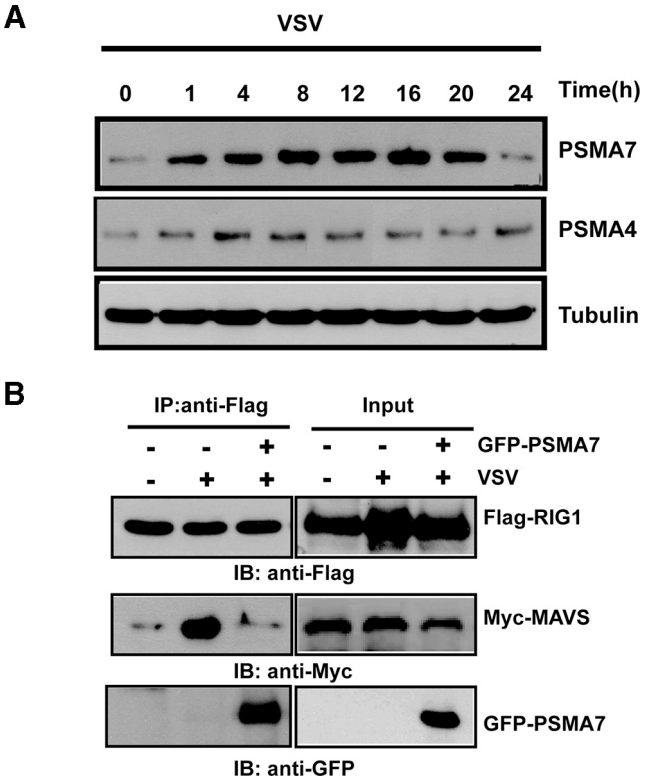

FIGURE 5. Regulation of PSMA7 during infection. *A*, MCF-7 cells were treated with VSV for indicated times. Cells were then harvested at different times after VSV infection. Whole cell lysates were analyzed by immunoblotting with anti-PSMA7, anti-PSMA4, or anti-β-Tubulin Ab. *B*, MCF-7 cells were infected with VSV virus for 1 h and then cotransfected with Flag-MAVS and Myc-RIG1 with or without the expression vector encoding GFP-PSMA7. Anti-Flag immunoprecipitate was analyzed by immunoblotting with anti-Myc, anti-GFP, or anti-Flag Ab.

degradation. Third, the knockdown of endogenous PSMA7 increased the cellular amount of MAVS and IFN-β induction, possibly due to a reduced contact with proteasome complex or decreased proteasome activity. Because PSMA4 knockdown cells showed normal IFN-β signaling, we suggest that the reduced contact of MAVS with the proteasome complex in PSMA7 siRNA cells contributes mainly to the enhanced IFN-β signaling. Fourth, up-regulation of PSMA7 protein in response to virus infection indicates that PSMA7 serves as a negative feedback molecule to attenuate the persistence of antiviral state, highlighting the biological significance of PSMA7-MAVS association as an important cellular regulatory control.

There have been several reports about cellular regulatory proteins and viral proteins that interact with subunits of the proteasome complex and participate in the proteasome-dependent regulation (28, 32). Because proteasome subunits can be exchanged with exogenous subunits in vivo and in vitro (29–31), the regulatory effect of the exogenous PSMA7 on MAVS may be due to the PSMA7-mediated recruitment of MAVS to the proteasome complex. Human hepatitis B virus X protein, another binding target of PSMA7, is also quickly degraded by the proteasome pathway, suggesting that PSMA7 may have a role in recruiting substrates to the proteasome complex.

The ubiquitin-proteasome system (UPS) displays an important quality control function. Alterations in the proteasome proteolytic pathway contribute to protein alterations associated with aging and, in fact, dysregulation of the UPS has been linked to several disease states including neurodegenerative diseases, malignancies, and inflammatory-related diseases (33–38). Strong preclinical data now exist, which supports the use of reversible proteasome inhibitors to treat a variety of disease states including cancer, autoimmune and inflammatory diseases, myocardial infarction, and ischemic brain injury (39–42). PSMA7, a subunit of proteasome complex might play an important, yet undefined, key roles in UPS-linked disease. In this study, we have demonstrated that PSMA7 is involved in the stability of MAVS, which thereby provides negative regulation of the innate antiviral response against infection by RNA viruses. Thus, PSMA7 might function to regulate host innate immune signaling by destabilizing MAVS and targeting of PSMA7 through approaches such as siRNA could enhance antiviral responses, which has broad implications for the treatment of viral associated diseases.

Acknowledgments

We acknowledge Zhijian Chen (University of Texas Southwestern Medical Center) and Cheng Cao for providing the MAVS and PSMA7 expression plasmid. We also acknowledge Zming Yu for great help in preparation of the manuscript.

Disclosures

The authors have no financial conflict of interest.

References

1. Theofilopoulos, A. N., R. Baccala, B. Beutler, and D. H. Kono. 2005. Type I interferons (α/β) in immunity and autoimmunity. *Annu. Rev. Immunol.* 23: 307–336.
2. Kawai, T., and S. Akira. 2006. Innate immune recognition of viral infection. *Nat. Immunol.* 7: 131–137.
3. Perry, A. K., G. Chen, D. Zheng, H. Tang, and G. Cheng. 2005. The host type I interferon response to viral and bacterial infections. *Cell Res.* 15: 407–422.
4. Akira, S., and K. Takeda. 2004. Toll-like receptor signaling. *Nat. Rev. Immunol.* 4: 499–511.
5. Meylan, E., and J. Tschopp. 2006. Toll-like receptors and RNA helicases:two parallel ways to trigger antiviral responses. *Mol. Cell* 22: 561–569.
6. Fritz, J. H., R. L. Ferrero, D. J. Philpott, and S. E. Girardin. 2006. Nod-like proteins in immunity, inflammation and disease. *Nat. Immunol.* 7: 1250–1257.
7. Inohara, N., and G. Nunez. 2003. NODs: intracellular proteins involved in inflammation and apoptosis. *Nat. Rev. Immunol.* 3: 371–382.
8. Inohara, N., M. Chamaillard, C. McDonald, and G. Nunez. 2005. NOD-LRR proteins: role in host-microbial interactions and inflammatory disease. *Annu. Rev. Biochem.* 74: 355–383.
9. Martinon, F., and J. Tschopp. 2005. NLRs join TLRs as innate sensors of pathogens. *Trends Immunol.* 26: 447–454.
10. Kumar, H., T. Kawai, H. Kato, S. Sato, K. Takahashi, C. Coban, M. Yamamoto, S. Uematsu, K. J. Ishii, and O. Takeuchi. 2006. Essential role of IPS-1 in innate immune responses against RNA viruses. *J. Exp. Med.* 203: 1795–1803.
11. Kato, H., S. Sato, M. Yoneyama, M. Yamamoto, S. Uematsu, K. Matsui, T. Tsujimura, K. Takeda, T. Fujita, and O. Takeuchi. 2005. Cell type specific involvement of RIG-I in antiviral response. *Immunity* 23: 19–28.
12. Kato, H., O. Takeuchi, S. Sato, M. Yoneyama, M. Yamamoto, K. Matsui, S. Uematsu, A. Jung, T. Kawai, and K. J. Ishii. 2006. Differential roles of MDA5 and RIG-I helicases in the recognition of RNA viruses. *Nature* 441: 101–105.
13. Kawai, T., K. Takahashi, and S. Sato. 2005. An adaptor triggering RIG-1 and Mda5-mediated type I interferon induction. *Nat. Immunol.* 6: 981–988.
14. Yoneyama, M., M. Kikuchi, and T. Natsukawa. 2004. The RNA helicase RIG-1 has an essential function in double-stranded RNA-induced innate antiviral responses. *Nat. Immunol.* 5: 730–737.
15. Seth, R. B., L. Sun, C. K. Ea, and Z. J. Chen. 2005. Identification and characterization of MAVS, a mitochondrial antiviral signaling protein that activates NF-κB and IRF3. *Cell* 122: 669–682.
16. Hiscott, J., R. Lin, P. Nakhaei, and S. Paz. 2006. MasterCARD: a priceless link to innate immunity. *Trends Mol. Med.* 12: 2–10.
17. Sun, Q., L. Sun, and H. H. Liu. 2006. The specific and essential role of MAVS in antiviral innate immune responses. *Immunity* 24: 633–642.
18. Qi, B., Y. Huang, D. Rowe, and G. Halliday. 2007. VISA: a pass to innate immunity. *J. Biol. Chem.* 39: 287–291.
19. Xu, L. G., Y. Y. Wang, and K. J. Han. 2005. VISA is an adaptor protein required for virus-triggered IFN-β signaling. *Mol. Cell* 19: 727–740.
20. Moore, C. B., D. T. Bergstralh, J. A. Duncan, Y. Lei, T. E. Morrison, A. G. Zimmermann, M. A. Accavitti-Loper, V. J. Madden, L. Sun, and Z. Ye. 2008. NLRX1 is a regulator of mitochondrial antiviral immunity. *Nature* 451: 573–579.
21. Voges, D., P. Zwickl, and W. Baumeister. 1999. The 26S proteasome: a molecular machine designed for controlled proteolysis. *Annu. Rev. Biochem.* 68: 1051–1068.
22. Coux, O., K. Tanaka, and A. L. Goldberg. 1996. Structure and functions of the 20S and 26S proteasomes. *Annu. Rev. Biochem.* 65: 801–847.
23. Varshavsky, A. 2005. Regulated protein degradation. *Trends Biochem. Sci.* 30: 283–286.

24. Voges, D., P. Zwickl, and W. Baumeister. 1999. The 26S proteasome:a molecular machine designed for controlled proteolysis. *Annu. Rev. Biochem.* 68: 1051–1068.
25. Glickman, M. H., and A. Ciechanover. 2002. The ubiquitin-proteasome proteolytic pathway: destruction for the sake of construction. *Physiol. Rev.* 82: 373–428.
26. Cho, S., Y. Choi, J. Kim, S. Jeong, J. Kim, S. Kim, and S. Ryu. 2001. Binding and regulation of HIF-1a by a subunit of the proteasome complex *PSMA7. FEBS Lett.* 498: 62–66.
27. Hu, Z., Z. Zhang, E. Doo, O. Coux, A. L. Goldberg, and T. J. Liang. 1999. Hepatitis B virus X protein is both a substrate and a potential inhibitor of the proteasome comoplex. *J. Virol.* 73: 7231–7240.
28. Huang, J., J. Kwong, E. C.-Y. Sun, and T. J. Liang. 1996. Proteasome complex as a potential cellular target of hepatitis B virus X protein. *J. Virol.* 70: 5582–5591.
29. Fruh, K., M. Gossen, K. Wang, H. Bujard, P. A. Peterson, and Y. Yang. 1994. Displacement of housekeeping proteasome subunits by MHC-encoded LMPs: a newly discovered mechanism for modulating the multicatalytic proteinase complex. *EMBO J.* 13: 3236–3244.
30. Voges, D., P. Zwickl, and W. Baumeister. 1999. The 26S proteasome: a molecular machine designed for controlled proteolysis. *Annu. Rev. Biochem.* 68: 1015–1068.
31. Borissenko, L., and M. Groll. 2007. 20S proteasome and its inhibitors: crystallographic knowledge for drug development. *Chem. Rev.* 107: 687–717.
32. Cortid, O., C. Hamped, N. Patengee, K. Vaupela, A. Yamamotof, M. Dichgansa, A. Briced, E. E. Wankerc, P. J. Kahlee, and T. Gassere. 2005. Parkin interacts with the proteasome subunit α4. *FEBS Lett*. 579: 3913–3919.
33. Kahle, P. J., and C. Haass. 2004. How does parkin ligate ubiquitin to Parkinson's disease? *EMBO Rep.* 5: 681–685.
34. Ben-Neriah, Y. 2002. Regulatory functions of ubiquitination in the immune system. *Nat. Immunol.* 3: 20–26.
35. Finley, D., A. Ciechanover, and A. Varshavsky. 2004. Ubiquitin as a central cellular regulator. *Cell* 116: S29–S32.
36. Hershko, A., and A. Ciechanover. 1998. The ubiquitin system. *Annu. Rev. Biochem.* 67: 425–479.
37. Liu, Y. C. 2004. Ubiquitin ligases and the immune response. *Annu. Rev. Immunol.* 22: 81–127.
38. Kumatori, A., K. Tanaka, N. Inamura, S. Sone, T. Ogura, T. Matsumoto, T. Tachikawa, S. Shin, and A. Ichihara. 1990. Abnormally high expression of proteasomes in human leukemia cells. *Proc. Natl. Acad. Sci. USA* 87: 7071–7075.
39. Fenteany, G., R. F. Standaert, W. S. Lane, S. Choi, E. J. Corey, and S. L. Schreiber. 1995. Inhibition of proteasome activities and subunit-specific amino-terminal threonine modification by lactacystin. *Science* 268: 726–731.
40. Kane, R. C., P. F. Bross, A. T. Farrell, and R. Pazdur. 2003. Velcade: U.S. FDA approval for the treatment of multiple myeloma progressing on prior therapy. *Oncologist* 8: 508–513.
41. Yang, H., D. Chen, Q. C. Cui, X. Yuan, and Q. P. Dou. 2006. Celastrol, a triterpene extracted from the Chinese "Thunder of God Vine," is a potent proteasome inhibitor and suppresses human prostate cancer growth in nude mice. *Cancer Res.* 66: 4758–4765.
42. Yang, H., G. Shi, and Q. P. Dou. 2007. The tumor proteasome is a primary target for the natural anticancer compound isolated from "Indian winter cherry". *Mol. Pharmacol.* 71: 426–437.

Repulsion of Superinfecting Virions: A Mechanism for Rapid Virus Spread

Virginie Doceul, *et al.*

Science **327**, 873 (2010);
DOI: 10.1126/science.1183173

Science (print ISSN 0036-8075; online ISSN 1095-9203) is published weekly, except the last week in December, by the American Association for the Advancement of Science, 1200 New York Avenue NW, Washington, DC 20005.

Repulsion of Superinfecting Virions: A Mechanism for Rapid Virus Spread

Virginie Doceul,* Michael Hollinshead,* Lonneke van der Linden,† Geoffrey L. Smith‡

Viruses are thought to spread across susceptible cells through an iterative process of infection, replication, and release, so that the rate of spread is limited by replication kinetics. Here, we show that vaccinia virus spreads across one cell every 75 minutes, fourfold faster than its replication cycle would permit. To explain this phenomenon, we found that newly infected cells express two surface proteins that mark cells as infected and, via exploitation of cellular machinery, induce the repulsion of superinfecting virions away toward uninfected cells. Mechanistically, early expression of proteins A33 and A36 was critical for virion repulsion and rapid spread, and cells expressing these proteins repelled exogenous virions rapidly. Additional spreading mechanisms may exist for other viruses that also spread faster than predicted by replication kinetics.

Mechanisms enhancing the cell-to-cell spread of intracellular pathogens are important for virulence and are targets for development of antimicrobial therapeutics. Vaccinia virus (VACV) is a poxvirus and is the live vaccine used to eradicate smallpox (*1*). VACV replication is unusual in that it produces both single- and double-enveloped virions (*2*, *3*). The single-enveloped virions, called intracellular mature virus (IMV), remain intracellular until cell lysis and spread slowly from cell to cell. In contrast, the double-enveloped virions, called cell-associated enveloped virus (CEV) and extracellular enveloped virus (EEV), are released rapidly and mediate efficient cell-to-cell spread and long-range dissemination (*3*, *4*). VACV spreading mechanisms include virus-induced cell motility (*5*) and the formation of actin projections (*6*–*8*) that propel VACV particles toward other cells late during infection (*9*). However, we wondered whether either mechanism could explain how VACV Western Reserve (WR) spreads rapidly to form a plaque of diameter 2.90 ± 0.07 mm (SEM, nine experiments, n = 11 to 12 plaques) in 3 days (Fig. 1A). The distance between nuclei of adjacent BSC-1 cells was 37.26 ± 1.02 μm (SEM, n = 25 single cells and the 5 to 8 cells in contact with it), so that VACV was spreading across each cell in <2 hours. To study this further, live video microscopy was used to measure the spread of VACV-induced cytopathic effect after infection with VACV WR (Fig. 1, B and C) or VACV expressing enhanced green fluorescent protein (EGFP) fused to core protein A5 that is expressed late during infection (vEGFPA5L) (Fig. 1, D to F, and movies S1 to S5) (*10*, *11*). A linear increase in plaque size with time was observed (Fig. 1G), and the mean rate of spread was 32.36 ± 0.74 μm/hour (SEM, n = 9 plaques) for VACV WR. Knowing the distance between nuclei of adjacent cells, this indicated that VACV crossed one cell every 1.2 hours. This rate of spread is inconsistent with VACV replication kinetics, in which new virions are formed only 5 to 6 hours after infection (*12*), or virus-induced cell motility, in which cells start to move 5 to 6 hours after infection (*5*). These observations demonstrated that another mechanism to accelerate spread must exist. Mutants defective in actin tail formation (ΔA36R, ΔA33R, ΔA34R, ΔB5R, ΔF13L, and ΔF12L) (*3*) spread much more slowly (Fig. 1, G and H), infecting only one cell every 5 to 6 hours, which is consistent with replication kinetics. This reaffirmed the importance of actin tails for VACV spread but did not explain the rapid dissemination because actin tails are produced only late during infection after new virions are formed.

Inspection of plaques formed by vEGFPA5L revealed EGFP-positive virions (green dots) several cells away from EGFP-positive cells, where virions are formed, showing that VACV particles spread rapidly to distal cells (Fig. 1F). To investigate this phenomenon, actin was stained with phalloidin, and confocal optical sections revealed virus-tipped actin tails on cells producing new virions but also on distal cells lacking virus factories and so not producing virions (no

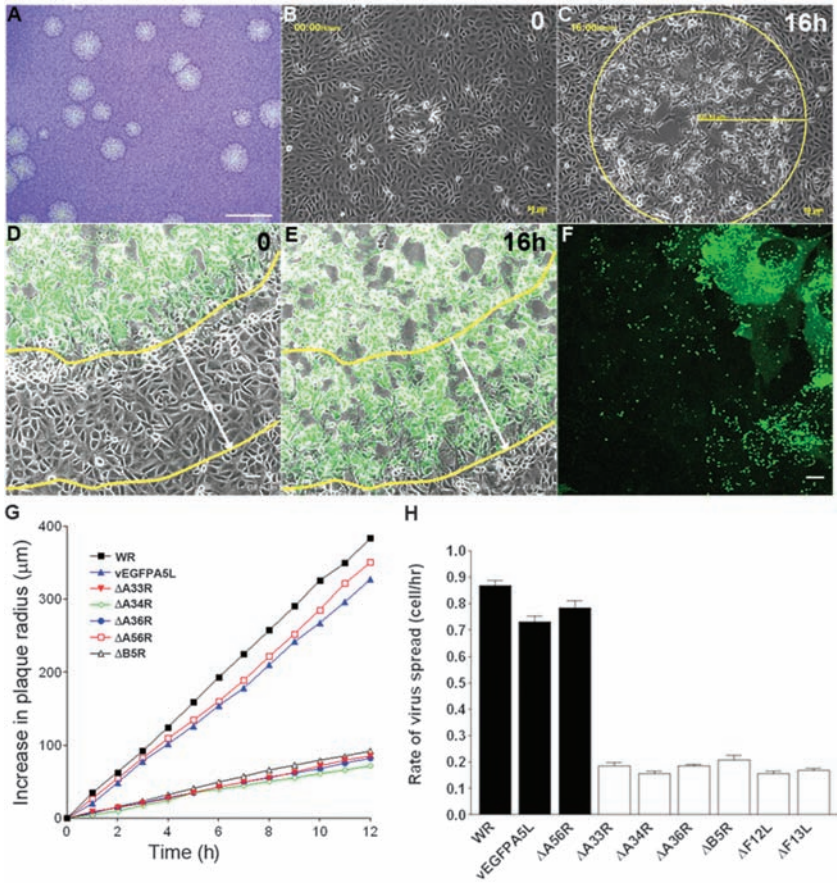

Fig. 1. VACV spreads more rapidly than predicted. (**A**) VACV plaques 3 days after infection in BSC-1 cells. Scale bar, 5 mm. (**B** and **C**) Live cell imaging recording plaque formation at 0 (B) and 16 (C) hours later. (**D** and **E**) Live cell imaging of vEGFPA5L-infected cells confirmed the correlation between cytopathic effect (cpe) and virus infection. Yellow lines indicate the boundary between infected and uninfected cells and white arrows indicate the distance this has moved over 16 hours. (**F**) Confocal image showing the spread of EGFP-tagged virus particles (single green dots) far from the center of infection. (**G**) Increase in plaque radius formed by VACV WR and mutants with time; n = 6 to 11 plaques. (**H**) Diagram showing the rate of spread (BSC-1 cell per hour) with indicated viruses. White bars indicate viruses with a defect in actin tail formation. Error bars are SEM, with n = 6 to 11 plaques. Scale bar, (A) 5 mm, (B) to (E) 50 μm, and (F), 10 μm.

Department of Virology, Faculty of Medicine, Imperial College London, St Mary's Campus, Norfolk Place, London W2 1PG, UK.

*These authors contributed equally to this work.
†Present address: Radboud University Nijmegen, Nijmegen Centre for Molecular Life Sciences, 6500 HB Nijmegen, The Netherlands.
‡To whom correspondence should be addressed. E-mail: geoffrey.l.smith@imperial.ac.uk

EGFP expression) (Fig. 2A). This result was reproduced in different cell lines (BSC-1, RK13, ECV, and CEF) and using different VACV strains (WR and Lister) (figs. S1 and S2). To be certain that actin tails on cells that lack virus factories were not derived from distant virus-producing cells, a lawn of cells was formed in which some cells expressed cherry fluorescent protein fused to actin (cherry-actin) and thus produced red actin tails after virus infection (Fig. 2B and movies S6 and S7). After infection of such monolayers at low multiplicity, cells containing green factories adjacent to a red cell (cherry-actin positive) were studied. This revealed green virions on tips of red actin tails originating from a red cell that lacked any green factory and therefore new virions. Careful examination of *z* stacks of these cells confirmed no virus factory was present. Therefore, the virions and actin tail originated from different cells. Further examination by means of time-lapse microscopy revealed virus-tipped red actin tails on a cell 5, 20, and 50 min before green factory formation (55 min) (Fig. 2B), confirming that actin tails appeared before virion production. Furthermore, virions on a red actin tail were observed recontacting the same red cell and inducing another actin tail (movie S7). Thus, virions can be repelled repeatedly, thereby accelerating spread until an uninfected cell is found.

To understand this mechanism, we searched for the required VACV proteins. Proteins K2 and A56 inhibit entry of IMV by binding the membrane fusion complex on the IMV surface (*13*–*15*), but this is masked on EEV or CEV, and mutants lacking these genes form normal-sized plaques (*16*, *17*). Better candidates would be early, cell-surface proteins that are needed for actin tail formation. Although proteins A33, A34, A36, B5, F12, and F13 are needed for efficient actin tail

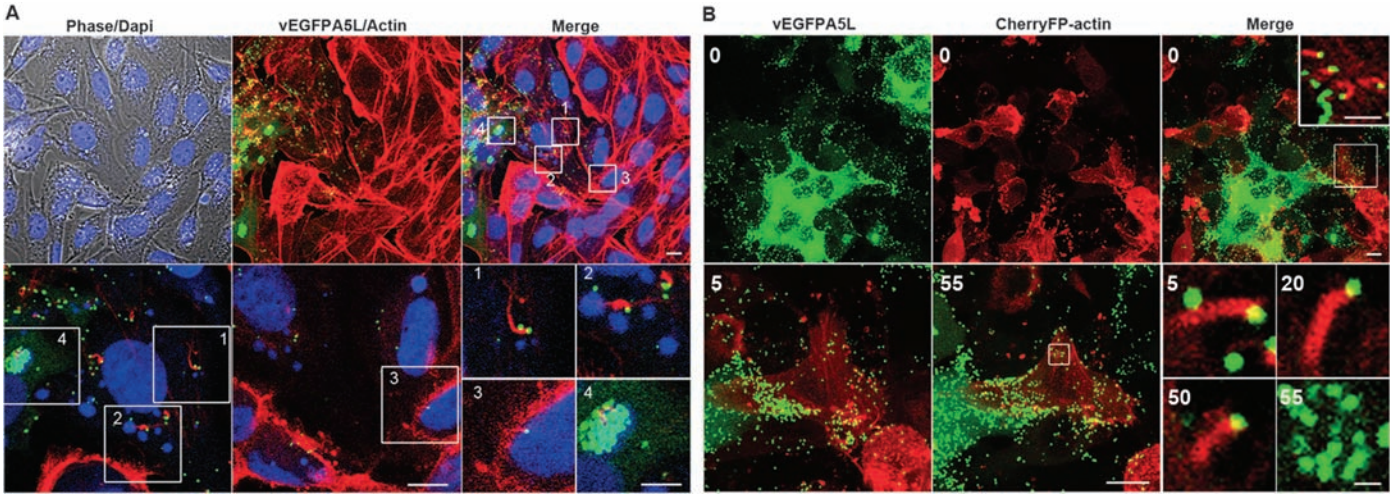

Fig. 2. Cells form actin tails before production of new virions. (**A**) Confocal images showing the edge of vEGFPA5L plaque (green) on BSC-1 cells stained for actin (red) or DNA (blue). Bottom panel shows zoomed areas (white squares 1 to 4). Actin tails are on cells with nascent factories (cytoplasmic blue) but that are not producing any virus particles (green) (squares 1 and 2), and on a cell with no virus factory (square 3), whereas square 4 shows a productive virus factory (green). Scale bars, top row, 10 μm; bottom row, 10 μm; and insets 1 to 4, 5 μm. (**B**) Actin tails (red) present at the surface of a cell expressing cherryFP-actin but with no green virus factory [time (*t*) = 0, white square and zoomed inset]. Bottom panels show zoomed images of this cell with actin tails detected 5, 20, and 50 min later, before the appearance of virus factories at 55 min as indicated by the white square. Scale bars, top row, 10 μm; top right inset, 5 μm; bottom row, 10 μm; and bottom right inset, 1 μm.

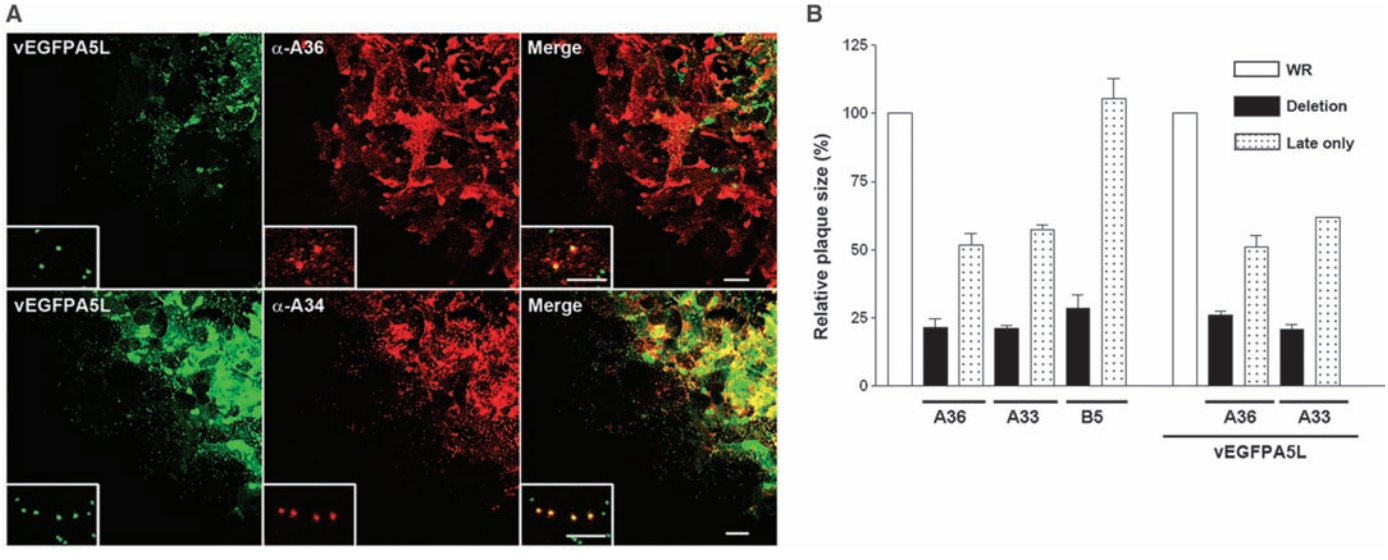

Fig. 3. Early expression of A33 and A36 is important for VACV spread. (**A**) Images of edge of plaque showing A36, but not A34, is expressed early during infection. A36 was detected in cells where no late protein A5 (green) was present, whereas A34 was expressed late during infection in cells that also express A5. (Insets) Zoomed images of virions (single green dots) relative to A36 and A34 distribution. (**B**) Graph showing the size of plaques formed by recombinant viruses in which *A33R*, *A36R*, or *B5R* are under a late promoter only (4b) or deleted (Δ) as compared with parental viruses WR or vEGFPA5L. Error bars are SEM mean values from three experiments with *n* = 11 to 12 plaques. Scale bars, 20 μm; insets, 5 μm.

formation, only surface proteins B5 (*18*), A33 (*19*), and A36 (*20*) are expressed early (and late). Immunostaining of plaques formed by vEGFPA5L demonstrated that A33 and A36 are expressed early during infection at the periphery of plaques before expression of late proteins (A34, EGFP-A5, and B5) (Fig. 3A and fig. S3). A34 and B5 were nevertheless detectable on virions spreading toward noninfected cells, as expected. Thus, A33 and A36 seemed candidates for early induction of actin tails.

The importance of early expression of A33 and A36 was investigated by generating recombinant viruses in which *A33R*, *A36R*, or *B5R* genes were driven only by a late promoter (*21*). Infection of cells by these viruses (v4b-A33, v4b-A36, and v4b-B5) confirmed expression of these proteins only late during infection (fig. S4) and showed that plaques formed by v4b-A33 and v4b-A36 were much smaller than wild type and closer to those formed by deletion mutants lacking either gene (Fig. 3B). In contrast, v4b-B5 formed plaques similar to wild type. Thus, early expression of A33 and A36, but not B5, is critical for efficient VACV spread. Similar results were obtained with viruses in which 4b-*A33R* and 4b-*A36R* were inserted into vEGFP-A5L, allowing direct visualization of spreading virions via EGFP. Virions released from cells infected by these viruses (vEGFPA5L/4b-A33 and vEGFPA5L/4b-A36) spread poorly as compared with vEGFPA5L and induced actin tails only on cells with a virus factory (fig. S5).

Next, we investigated whether A33 and A36 are sufficient to induce actin tails upon contact with an EEV particle. Both proteins are expressed on the plasma membrane of VACV-infected cells (*22*–*24*) and interact with each other (*25*–*27*). Lentivirus vectors expressing A33 or A36 fused to a C-terminal V5 tag were used to generate HeLa cells expressing cell surface A33-v5, A36-v5, or A36-v5 and A33-v5 (Fig. 4A and fig. S6). These cells were incubated with EEV particles and then stained with phalloidin and a monoclonal antibody to B5. Actin tails were detected on cells expressing A33-v5 and A36-v5 within 15 to 30 min (Fig. 4, B and C). Similar results were obtained with haemagglutinin (HA)–tagged A33. No actin tails were detected if only one protein was expressed or if the cells were incubated with IMV or with GFP-tagged herpes simplex virus 1 (HSV-1). Thus, A33 and A36 are both necessary and sufficient to induce actin tails after binding EEV particles. Currently, we are investigating the effect of ectopic expression of A33 and A36 on VACV spread by measuring plaque size using additional cell lines that form clearer plaques.

Here, we demonstrate that VACV has evolved a mechanism (Fig. 4D) by which infected cells repel superinfecting CEV/EEV particles on actin tails toward neighboring cells. Two outcomes are then possible: (i) If the neighboring cell is uninfected, the virion enters and starts a new cycle of replication; (ii) alternatively, if the cell is already infected then superinfection is blocked, and a new actin tail is formed, propelling the virus further away until it reaches uninfected cells. This mechanism accelerates virus spread and explains how VACV can cross one cell every 1.2 hours as determined by means of live cell imaging. Early expression of proteins A33 and A36 is required, and viruses expressing either protein only late during infection form small plaques. These plaques are closer in size to those formed by the deletion mutants lacking either gene than to wild type, indicating that the formation of actin tails upon superinfection is more important for virus spread than the production of actin tails on cells releasing new virions. All mutations that cause VACV strains to spread poorly and form small plaques also cause dramatic attenuation in vivo, showing the biological importance of rapid spread for VACV virulence (*18*, *20*, *28*, *29*).

Plaque assays were first described more than 50 years ago (*30*), and many animal viruses form plaques of size comparable with VACV. Some of these viruses, for instance HSV-1 (*31*), have replication kinetics similar to VACV, suggesting that other viruses also spread faster than predicted by their replication kinetics. The mechanisms underlying cell-to-cell spread of many viruses remain

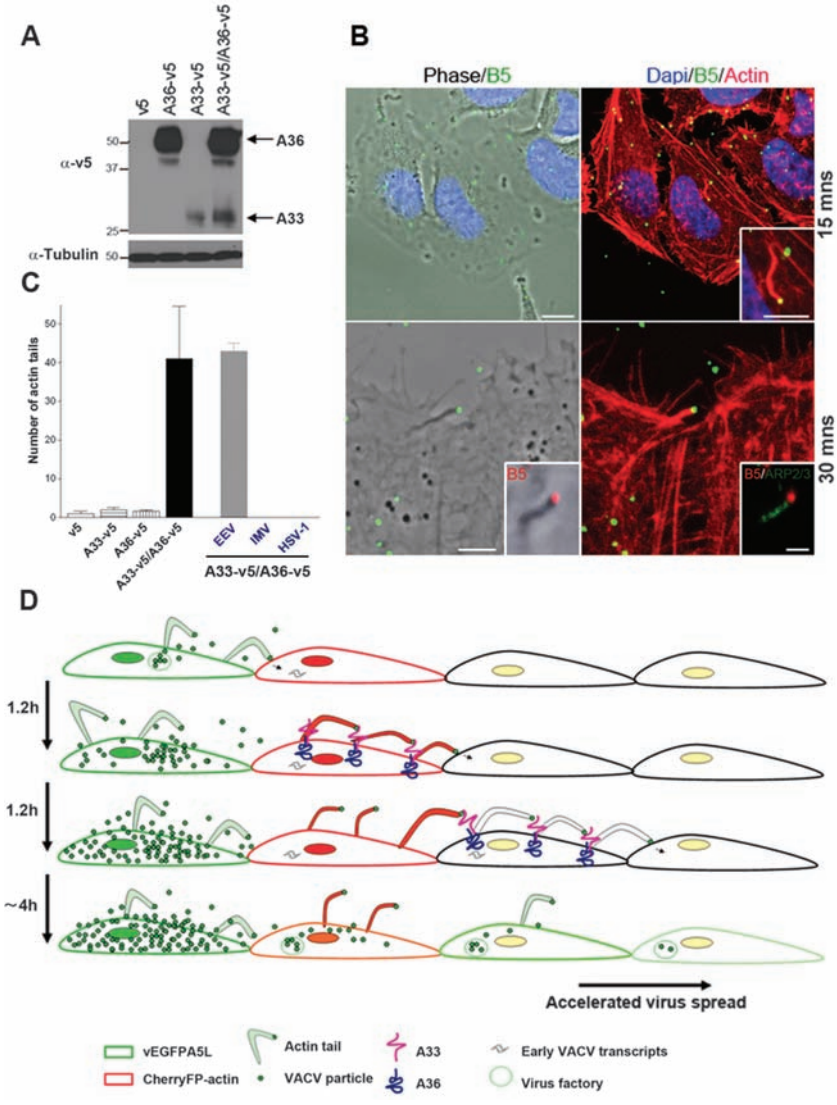

Fig. 4. Expression of A33 and A36 is sufficient for actin tail formation. (**A**) Immunoblot showing A33 and A36 expression. (**B**) Actin tails present 15 and 30 min after spinoculation of EEV particles onto HeLa cells expressing A33 and A36 proteins. Staining for Arp2/3 shows actin polymerisation machinery. Scale bars, top row, 10 μm; inset, 5 μm; bottom row, 5 μm; inset, 1 μm. (**C**) Graph showing the mean number of actin tails detected per coverslip in the different cell lines. Actin tails were not formed by IMV or HSV-1. Error bars are SEM; $n = 3$ experiments. (**D**) Model showing how VACV spreads rapidly. The first infected cell expresses EGFP-A5 late during infection and releases green virions, which infect an adjacent cell expressing cherry actin (red). Early after infection, A33 and A36 are expressed at the cell surface and mark the cell as infected. Upon contact with new CEV/EEV particles, the A33/A36 complex induces the formation of red actin tails, which repel these virions toward uninfected cells. Superinfecting virions may be repelled from multiple infected cells before an uninfected cell is found that can be infected.

poorly understood, and the elucidation of such mechanisms could lead to the discovery of novel therapeutics.

References and Notes

1. B. Moss, in *Fields Virology*, D. M. Knipe, Ed. (Lippincott Williams & Wilkins, Philadelphia, 2007), vol. 2, pp. 2905–2946.
2. R. C. Condit, N. Moussatche, P. Traktman, *Adv. Virus Res.* **66**, 31 (2006).
3. G. L. Smith, A. Vanderplasschen, M. Law, *J. Gen. Virol.* **83**, 2915 (2002).
4. K. L. Roberts, G. L. Smith, *Trends Microbiol.* **16**, 472 (2008).
5. C. M. Sanderson, M. Way, G. L. Smith, *J. Virol.* **72**, 1235 (1998).
6. R. Blasco, N. B. Cole, B. Moss, *J. Virol.* **65**, 4598 (1991).
7. G. Hiller, K. Weber, L. Schneider, C. Parajsz, C. Jungwirth, *Virology* **98**, 142 (1979).
8. G. V. Stokes, *J. Virol.* **18**, 636 (1976).
9. S. Cudmore, P. Cossart, G. Griffiths, M. Way, *Nature* **378**, 636 (1995).
10. G. C. Carter *et al.*, *J. Gen. Virol.* **84**, 2443 (2003).
11. Materials and methods are available as supporting material on *Science* online.
12. L. G. Payne, K. Kristenson, *J. Virol.* **32**, 614 (1979).
13. P. C. Turner, R. W. Moyer, *Virology* **380**, 226 (2008).
14. T. R. Wagenaar, B. Moss, *J. Virol.* **81**, 6286 (2007).
15. T. R. Wagenaar, B. Moss, *J. Virol.* **83**, 1546 (2009).
16. K. M. Law, G. L. Smith, *J. Gen. Virol.* **73**, 549 (1992).
17. M. Law, R. Hollinshead, G. L. Smith, *J. Gen. Virol.* **83**, 209 (2002).
18. M. Engelstad, G. L. Smith, *Virology* **194**, 627 (1993).
19. R. L. Roper, E. J. Wolffe, A. Weisberg, B. Moss, *J. Virol.* **72**, 4192 (1998).
20. J. E. Parkinson, G. L. Smith, *Virology* **204**, 376 (1994).
21. J. Rosel, B. Moss, *J. Virol.* **56**, 830 (1985).
22. M. M. Lorenzo, I. Galindo, G. Griffiths, R. Blasco, *J. Virol.* **74**, 10535 (2000).
23. R. L. Roper, L. G. Payne, B. Moss, *J. Virol.* **70**, 3753 (1996).
24. H. van Eijl, M. Hollinshead, G. L. Smith, *Virology* **271**, 26 (2000).
25. B. Perdiguero, R. Blasco, *J. Virol.* **80**, 8763 (2006).
26. S. Röttger, F. Frischknecht, I. Reckmann, G. L. Smith, M. Way, *J. Virol.* **73**, 2863 (1999).
27. E. J. Wolffe, A. S. Weisberg, B. Moss, *J. Virol.* **75**, 303 (2001).
28. A. A. McIntosh, G. L. Smith, *J. Virol.* **70**, 272 (1996).
29. W. H. Zhang, D. Wilcock, G. L. Smith, *J. Virol.* **74**, 11654 (2000).
30. R. Dulbecco, *Proc. Natl. Acad. Sci. U.S.A.* **38**, 747 (1952).
31. G. Elliott, P. O'Hare, *J. Virol.* **73**, 4110 (1999).

32. We thank Professor Rick E. Randall, University of St. Andrews for the lentivirus vectors. GLS is a Wellcome Trust Principal Research Fellow. This work was supported by the UK Medical Research Council.

Supporting Online Material

www.sciencemag.org/cgi/content/full/science.1183173/DC1
Materials and Methods
Figs. S1 to S6
References
Movies S1 to S7

12 October 2009; accepted 8 January 2010
Published online 21 January 2010;
10.1126/science.1183173
Include this information when citing this paper.

Drive Against Hotspot Motifs in Primates Implicates the *PRDM9* Gene in Meiotic Recombination

Simon Myers,[1,2]*† Rory Bowden,[1,2]* Afidalina Tumian,[1] Ronald E. Bontrop,[3] Colin Freeman,[2] Tammie S. MacFie,[4]‡ Gil McVean,[1,2]§ Peter Donnelly[1,2]§

Although present in both humans and chimpanzees, recombination hotspots, at which meiotic crossover events cluster, differ markedly in their genomic location between the species. We report that a 13–base pair sequence motif previously associated with the activity of 40% of human hotspots does not function in chimpanzees and is being removed by self-destructive drive in the human lineage. Multiple lines of evidence suggest that the rapidly evolving zinc-finger protein PRDM9 binds to this motif and that sequence changes in the protein may be responsible for hotspot differences between species. The involvement of PRDM9, which causes histone H3 lysine 4 trimethylation, implies that there is a common mechanism for recombination hotspots in eukaryotes but raises questions about what forces have driven such rapid change.

In humans and most other eukaryotes, meiotic crossover events typically cluster within narrow regions termed hotspots (*1*–*5*). Previously (*6*), we identified a degenerate 13–base pair (bp) motif, CCNCCNTNNCCNC, that is overrepresented in human hotspots. Both linkage disequilibrium (LD)–based analysis (*6*) and sperm typing at currently active hotspots (*7*) implicated this motif in the activity of 40% of hotspots.

Despite nearly 99% identity at aligned bases, humans and chimpanzees show little if any sharing of hotspot locations (*4*, *5*), although it has remained undetermined whether the recently identified hotspot motif is also active in the chimpanzee. To resolve this question, we collected chimpanzee genetic variation data at 22 loci where there is both an inferred hotspot at the orthologous location in humans and human-chimpanzee sequence conservation of the 13-nucleotide oligomer: 16 motifs within THE1 elements and 6 within L2 elements, chosen for their high activity of a particular "core" version of the motif in humans (fig. S1). We used the statistical software LDhat to estimate recombination rates separately in each region in different populations of both species (*8*). For humans, we used the Haplotype Map (HapMap) Phase II data. For chimpanzees, we genotyped 36 Western, 20 Central, and 17 Vellorosus chimpanzees at a total of 694 chimpanzee single-nucleotide polymorphisms (SNPs), an average of 31.5 per region.

Because these regions are inferred human hotspots, the average estimated recombination rate surrounding the motif in humans showed a strong peak for both L2 and THE1 elements (Fig. 1A). In contrast, chimpanzees showed no evidence of increased recombination rates for either background. In Western chimpanzees, the THE1 estimated recombination rate around the motif was similar to the regional average, whereas a weak peak in mean rate for the L2 elements was produced solely by a single potential hotspot in one of the six regions (Fig. 1B). Results for the other chimpanzee subspecies were less informative (fig. S2) (*8*) but did not reveal a different pattern. To ensure that unknown haplotypic phase, smaller sample size, less dense data, and SNP ascertainment in chimpanzees had not compromised the ability to detect hotspots, we repeatedly sampled from the Centre d'Etude du Polymorphisme Humain (CEPH) from Utah (CEU) HapMap population data to produce human data sets comparable with those from chimpanzees in terms of these features (*8*). We conditioned only on the presence of the 13-nucleotide oligomer in THE1 and L2 elements and not the presence of a hotspot. This bootstrap technique revealed that the differences between human and chimpanzee rates cannot be explained by differences in power ($P = 0.00052$), although the signal was only significant for THE1 elements when analyzed separately ($P = 0.00012$) (fig. S3). These results provide evidence that the 13-nucleotide oligomer motif does not recruit hotspots in chimpanzees, implying changes in recombination machinery between humans and chimpanzees. The existence of factors capable of such changes in recombination genome-wide has been demonstrated in *Caenhabditis elegans* (*9*) and by the mapping in mice of a trans-acting factor responsible for differences in hotspot location among inbred strain crosses (*10*, *11*).

[1]Department of Statistics, Oxford University, 1 South Parks Road, Oxford OX1 3TG, UK. [2]Wellcome Trust Centre for Human Genetics, Oxford University, Roosevelt Drive, Oxford OX3 7BN, UK. [3]Department of Comparative Genetics and Refinement, Biomedical Primate Research Center, Lange Kleiweg 139 2288 GJ, Rijswijk, Netherlands. [4]Department of Zoology, University of Cambridge, Downing Street, Cambridge CB2 3EJ, UK.

*These authors contributed equally to this work.
†To whom correspondence should be addressed. E-mail: myers@stats.ox.ac.uk
‡Present address: Institute of Cell and Molecular Science, Barts and The London School of Medicine and Dentistry, 4 Newark Street, London E1 2AT, UK.
§These authors contributed equally to this work.